HHS Public Access

Author manuscript

Magn Reson Med. Author manuscript; available in PMC 2016 May 20.

Published in final edited form as:

Magn Reson Med. 2015 March ; 73(3): 921–928. doi:10.1002/mrm.25208.

Reproducibility and reliability of short-TE whole brain MR spectroscopic imaging at 3T

Xiao-Qi Ding[1,*], **Andrew A. Maudsley**[2], **Sulaiman Sheriff**[2], **Paulo R. Dellani**[1], and **Heinrich Lanfermann**[1]

[1]Institute of Diagnostic and Interventional Neuroradiology, Hannover Medical School, Hannover, Germany

[2]Department of Radiology, University of Miami School of Medicine, Miami, FL, USA

Abstract

Purpose—A feasibility study of a short TE EPSI that trades off sensitivity, compared with other short-TE methods, to achieve whole brain coverage, using inversion recovery and spatial oversampling to control lipid bleeding.

Methods—Twenty subjects were scanned to examine inter-subject variance. One subject was scanned 5 times to examine intra-subject reproducibility. Data were analyzed to determine coefficients of variance (COV) and intra-class correlation coefficient (ICC) for N–acetylaspartate (NAA), total creatine (tCr), choline (Cho), glutamine/glutamate (Glx) and myo-inositol (ml). Regional metabolite concentrations were derived by using multi-voxel analysis based on lobar level anatomic regions.

Results—For whole brain mean values the intra-subject COVs were 14%, 15%, and 20% for NAA, tCr, and Cho respectively, and 31% for Glx and ml. The inter-subject COVs were up to 6% higher. For regional distributions the intra-subject COVs were ≤ 5% for NAA, tCr, Cho, ≤ 9% for Glx, and ≤15% for ml, with about 6% higher inter-subject COVs. The ICCs of 5 metabolites were ≥ 0.7, indicating the reliability of the measurements.

Conclusion—The present EPSI method enables estimation of the whole brain metabolite distributions including Glx and ml with small voxel size, and a reasonable scan time and reproducibility.

Keywords

whole brain MR spectroscopic imaging; short echo time; short acquisition time; glutamine/glutamate; myo-inositol

[*]**Corresponding author:** Xiao-Qi Ding, Institute of Diagnostic and Interventional Neuroradiology, Hannover Medical School, Carl-Neuberg-Str. 1, 30625 Hannover, Germany, Tel.: 0049 511 532 3401xiaoqi, Fax: 0049 511 532 5876.

Conflicts of interest and source of Funding: None

Introduction

Proton magnetic resonance spectroscopy (^{1}H-MRS) can be used in vivo to detect cerebral metabolites such as N-acetyl-aspartate (NAA), total creatine (tCr), total choline (tCho), glutamine (Gln) and glutamate (Glu), and myo-inositol (ml), and is being increasingly used for clinical studies (1). However, vendor-provided acquisition techniques of single voxel MRS (SVS) or volume-selected spectroscopic imaging (MRSI) suffer from limited spatial coverage, which continues to limit clinical use. Therefore, a challenge for clinical applications is to develop MR spectroscopic imaging (MRSI) techniques to achieve whole brain (wb) coverage with good spatial resolution and within scan times suitable for patient studies.

Whole-brain MRSI has three primary considerations that can impact spectral quality and reproducibility. First, methods using volume selection or saturation to avoid subcutaneous lipid contamination cannot be used without impacting neighboring brain tissue. Second, data must be obtained from a large volume of the brain, which impacts the achievable B0 homogeneity and thereby the spectral quality and water suppression. Third, consideration must be paid to obtaining whole-brain spatial information at sufficiently high spatial resolution within acceptable acquisition times. Previous work towards these requirements includes the use of an inversion-recovery preparation for lipid nulling (2), which enables spectra to be obtained from cortical surface areas. While this also incurs some loss of sensitivity for the metabolite resonances (3,4), this can be offset by using shorter TEs, which are made possible by the use of a simple spin-echo excitation, and some improvement in spectral quality resulting from reduced macromolecular contributions. Additional developments include high-speed MRSI methods (5–8), which enable all spatial information to be obtained within acceptable times; however, these techniques also have increased complexity relative to fully phase-encoded MRSI that can impact quality and reproducibility. An additional development is the use of parallel imaging acquisition and spectroscopic reconstruction (9–12), which obtains further reduction in acquisition time, albeit with some reduction of signal-to-noise (SNR) (13). However, it is possible that the impact of this SNR loss can be minimized by using shorter TEs and increasing the number of receiver channels to improve detection sensitivity.

wbMRSI has been reported for TE of 144 ms and spiral spatial-spectral readout (5,12,14) and for TE of 70 ms with echo-planar readout (15), with evaluation of the major singlet resonances from NAA, tCho, and tCr. However, potential information from combined glutamate and glutamine signal (Glx), and ml, which are best observed at short TE values, is of interest for a number of pathological processes. Several previous reports have described the implementation of short TE MRSI techniques (16–21); most of them used volume selection methods for scanning of a limited brain region. In this study a short TE EPSI technique with parallel imaging acquisition have been evaluated for the purpose of mapping regional concentrations of NAA, tCho, Cr, Glx, and ml in the whole human brain.

Methods

Ten healthy males aged 29 ± 3 years and ten healthy females aged age 27 ± 2 years underwent MR examinations for estimation of inter-subject reproducibility. One male (26 years old) was scanned at 5 separate occasions for assessment of intra-subject reproducibility. The study was approved by local Institution Review Board and written consent was obtained before the examinations. Studies were carried out at 3T (Verio, Siemens, Erlangen) with a twelve-channel phased-array head coil. The protocol included EPSI (TR/TE = 1550/17.6 ms) with parallel imaging acquisition and GRAPPA reconstruction – a 2×3 kernel size was used – and an acquisition time of 16 min (13). The parallel imaging acquisition was performed in one dimension, with a total of 32 k-space samples and complete sampling of the center 14 k-space lines, resulting in an acceleration factor of ~1.6. After correction for oversampling in the readout spatial and spectral dimensions the resultant image were equivalent to 50×50 voxels in-plane and 18 slices, over a field-of-view (FOV) of 280×280×180 mm, with selection of a slab of 140 mm covering the whole brain. The spatial sampling acquired data at a higher spatial resolution than warranted from sensitivity considerations in order to maximize spatial coverage via minimization of intra-voxel magnetic-susceptibility induced spectral distortions (4,22). Following spatial smoothing the effective voxel volume was approximately 1 ml. The acquisition included a second dataset obtained in an interleaved manner without water suppression and using 10° excitation and gradient-echo observation. This data provided a water reference signal with identical spatial parameters as the metabolite MRSI that was used for several processing functions and for normalization of the metabolite concentrations. In addition an axial T1-weighted 3D MPRAGE (Magnetization Prepared Rapid Gradient Echo) acquisition was obtained at 1 mm isotropic resolution (TR/TE/TI=1900/2.9/900 ms, flip angle 9°, acceleration factor = 2) with an acquisition time of 5 min. Both EPSI and MPRAGE were obtained with the same angulation.

Metabolite image reconstruction was carried out using the MIDAS (Metabolic Imaging and Data Analysis System) package, which has been described previously (15,23,24). Parametric spectral analysis was used to determine volumetric maps of NAA, tCr, tCho, Glx, and ml, which were interpolated to 64 × 64 × 32 points. The processing also included calculation of the relative tissue volume contribution to each MRSI voxel, by applying a tissue segmentation procedure to the T1-weighted MPRAGE data to map grey matter (GM), white matter (WM) and cerebrospinal fluid (CSF), followed by a resampling and convolution by the MRSI spatial response function to coincide with the MRSI voxel volume and location. All resultant maps were then spatially transformed and interpolated to a standard spatial reference (25) at 2 mm isotropic resolution, which was associated with a brain atlas that mapped the individual brain lobes and the cerebellum.

Maps of the mean and standard deviation (SD) for each metabolite in standard space, averaged from 5 repeated scans (intra-subject) and from 20 different subjects (inter-subjects) respectively, were then generated, and from these the maps of corresponding coefficient of variation (COV) were derived. Correction for CSF volume contribution was applied as $Met' = Met/(1-f_{csf})$ for $0 < f_{csf} < 0.3$, where Met is the uncorrected metabolite value and f_{csf} is the fraction of CSF in the MRSI voxel. After tests with different thresholds of linewidth

(LW) a maximum value of 11 Hz was chosen so that voxels with LW greater than 11 Hz, or a voxel tissue fraction (total of grey-matter and white-matter) of less than 70% were excluded from the calculation. Mean COVs over all voxels that remained after the above tests were then calculated together with the mean values of the relative metabolite signals by using voxel-based analysis. Mean regional metabolite distributions over different brain regions with associated intra-subject COVs or inter-subject COVs were derived by using multi-voxel analysis based on atlas-defined lobar anatomic regions, which identified nine anatomical regions: The frontal lobe left (LFL) and right (RFL), the temporal lobe left (LTL) and right (RTL), the parietal lobe left (LPL) and right (RPL), the occipital lobe left (LOL) and right (ROL), and the cerebellum (Cbl) (25). Metabolite concentrations were estimated with reference to the tissue water, and reported in institutional units (i.u.).

Regional distributions of each metabolite were estimated using paired t-tests for differences between left and right lobe ($\alpha = 0.05$), and two sided t-tests with Bonferroni correction for differences between male and female groups ($\alpha = 0.05/9 = 0.006$). Reproducibility of the measurements was estimated by using COV, defined as standard deviation of the difference between measurements divided by the mean values from the measurements. The intra-subject COV indicated changes over repeated measurements within a single subject, and the inter-subject COV indicated the variability across subjects. Measurement reliability of each metabolite was examined by intra-class correlation coefficient (ICC), which is the ratio of the variance of inter-subject metabolite distributions to the summation of the variance of inter-subject metabolite distributions, the variance of within subject metabolite distributions and the contribution of noise. Values of ICC near unity indicate that measurements yielded consistent results, while values near 0.5 and lower indicate that measurements are unreliable. All the statistical analyses were made using SPSS 21.

Results

Metabolite images

In Figure 1 are shown example metabolite maps of NAA, tCho, tCr, Glx, and ml (Fig. 1a) before spatial normalization to standard space. Also shown are multiple single-voxel spectra corresponding to the final spatial resolution of approximately 1 ml volume (Fig. 1b), and averaged spectra from 8 voxels of WM and GM at right parietal lobe (Fig. 1c), where the GM/WM showed clear difference in the spectral patterns. In Figure 2 are shown mean-value maps from five repeated scans (Fig. 2a) and the resultant COV maps (Fig. 2b). Note that these maps cover a smaller spatial extent due to the voxel exclusions.

Mean metabolite values averaged over the whole brain

In Table 1 (Top) are shown the mean metabolite concentrations averaged from 5 repeated scans and the corresponding intra-subject COVs. The values were derived with spectral LW thresholds ranging from 8 to 13 Hz in order to estimate resultant variability. These values indicate that increasing the LW threshold from 8 to 11 Hz resulted in little increase of mean COV (< 2%), while a LW threshold of 13 Hz resulted in an increase of up to 10%. As shown in Fig. 2b the mean COV values of NAA, tCho, and tCr were lower (≤ 20%) than those of ml and Glx (up to 31%). The COVs of the tissue segmentations, tissue water and linewidth are

also shown in Table 1, where the small COV for the tissue water indicates that this measurement provides a reliable reference for normalization of the metabolite signal. In Table 1 (Bottom) are shown the whole brain mean metabolite values from 20 healthy volunteers, and the associated inter-subject COVs with different LW thresholds. No significant differences were observed between results of the male and female groups ($p > 0.05$) for all lobes, therefore their results are presented together. Similar to the intra-subject values, an increase of LW threshold from 8 Hz to 11 Hz resulted in little increase of mean COV (< 3%) while an increase of LW from 8 to 13 Hz resulted in an increase of up to 18%. For this reason LW = 11 Hz was chosen as threshold for all further calculations. Again, the COV values of NAA, tCho, and tCr are lower (≤ 25%) than those of with small signal amplitude (ml and Glx, up to 38%), and the tissue water showed a low COV of 7%. Altogether, the inter-subject COVs of the metabolites were up to 6% higher than those of intra-subject.

Regional brain metabolite estimation

In Supplementary Table S1 (Top) are shown the mean regional brain metabolite concentrations averaged from five repeated scans, together with corresponding intra-subject COVs, and in Table 2 (Bottom) the corresponding values averaged for twenty healthy volunteers and the inter-subject COVs, as well as segmented brain tissues and linewidths. Paired t-tests showed significant differences of tCho between left and right lobes ($p = 0.02 – 0.03$), therefore the values of right and left lobe were not combined for further analyses. Both intra- and inter-subject mean metabolite concentrations showed clear regional differences that in cerebrum NAA value was higher while values of tCr, tCho, and ml were lower than those in cerebellum, except for Glx, which showed comparable concentrations in both brain structures (Fig. 3). These regional metabolite analyses revealed that the intra-subject COVs were up to 5% for NAA, tCr, tCho, up to 9% for Glx, and up to 15% for ml (15% for frontal lobe and up to 7% for other regions), respectively. The inter-subject COVs were up to 10% for NAA, tCr, tCho, up to 11% for Glx, and up to 13% for ml, respectively (Table S1). By using linear regression against the normalized GM fraction and extrapolating to 100% GM or zero (pure WM) metabolite concentrations in pure GM and pure WM were also generated and are shown in Table 2, where ICCs (≥ 0.7) for 5 metabolites were also given.

Discussion

Previous wbMRSI studies have been mostly limited to detect major singlet resonances from NAA, tCho, and tCr at medium to long TE values. However, information from Glx and ml is of interest for a number of pathological processes, since Glx reflects concentration of neurotransmitter glutamate and ml functions as glial cell marker and osmolyte (26). This is the first feasibility study using a methodology that trades off sensitivity, compared with other short-TE methods, to achieve whole brain coverage by using inversion recovery and spatial oversampling to control lipid bleeding. While the impact on the inversion-nulling approach for lipid suppression on the SNR for the singlet resonances has been presented for studies done at 1.5 T (3), this remains to be characterized for the Glx and ml resonances and 3 T. An alternative approach to reduce lipid signals is by using frequency-selective excitation

techniques, which ideally would not impact the SNR of metabolites investigated in this study (27); however, such techniques cannot be effectively implemented in the presence of the range of B0 inhomogeneity typically encountered with whole-head imaging. An additional sequence modification used in this study has been the incorporation of parallel-imaging methods to reduce acquisition times. Both of these sequence modifications have a counteracting impact on the spectral SNR relative to that of previous implementations, while additionally introducing increased complexity of the spectral analysis and a potential for increased signal contamination from subcutaneous lipid signals. The net result indicates that some degradation of performance was observable relative to a previous intra-subject study carried out using a 26 minute acquisition with a TE of 70 ms for mapping of NAA, tCho, and tCr, where the intra-subject COV of the whole brain NAA and tCr was found to be under 10%, and that of tCho in the order of 15% (15). In comparison, the present study found values for NAA and tCr of 13% to 15%, and ~20% for tCho, which suggests increased variability due to some reduction of the SNR or increased complexity of the spectral fitting. However, the ICCs for all metabolites were ≥ 0.7, indicating the reliability of the measurements.

This study demonstrated differences in the regional metabolite distributions over atlas-defined lobar anatomic regions. The regional analysis is clinically applicable since it could be used for estimation of local pathological changes. The regional COVs (Tables S1) indicate that changes of NAA, tCr, and tCho over 9%, Glx over 10% and ml over 15% would be detectable, which are consistent with the results of a SVS reliability study of Mullins et al. (28), with the difference that our Glx were slightly less than Mullins et al. found, that could be caused by sensitivity loss for J-coupled metabolites due to higher spatial resolution and/or lipid suppression. Our regional metabolite concentrations can also be compared to values published by Pouwels et al. (29) using SVS which remains the most widely used technique for clinical MRS studies. The authors reported measurements in a healthy volunteer group with the data being analyzed with software LCModel (30). Our observations that NAA value in cerebrum was higher than that in cerebellum, while values of tCr, tCho, and ml in cerebrum were lower than those in cerebellum, and Glx showed comparable concentrations in both, are consistent with the SVS results of Pouwels et al., who also found that the concentration of NAA in voxels of cerebral GM and WM was higher than that in cerebellum, while Cr, Cho, and ml in voxels of cerebral GM and WM were lower than those in cerebellum, with comparable cerebral and cerebellar concentration of Glx. Moreover, the present estimated regional metabolite concentrations are similar to those published by other groups (31,32). For example, a multicenter study of absolute quantification of NAA, tCho, and tCr (in reference to internal water) in volunteers aged 20–35 years showed the results of NAA (10.0±3.4 mM), tCho (1.9±1.0 mM), and tCr (6.5±3.7 mM) that are similar to our results (Tables 2) (31). Our results derived for pure GM and WM of frontal and parietal lobes that the concentrations of NAA, tCr, Glx and ml in GM were higher than those in WM while tCho in both were comparable, were qualitatively consistent to those of 2D MRSI (TR/TE= 1500/40ms) measurements on volunteers at 3T published by Gasparovic et al. (20), who studied cerebrum of a 15 mm slice containing part of frontal and parietal lobes, and used LCmodel analysis to estimate metabolite concentrations in relation to internal water. Differences from our findings are much larger differences between

metabolite concentrations in pure GM and in pure WM for tCr, Glx and ml. Beside the possible sensitivity loss for Glx mentioned above, reason could include differences in TE and region selection, since Gasparovic et al. (20) studied a central brain volume instead of the whole lobes. A study by Wiedermann et al. (17) that measured metabolite concentrations over a larger brain volume (three slices with a thickness of 15 mm for each) also found quite small differences between metabolite concentrations in pure GM and WM for tCr and ml.

In conclusion, with a clinically reasonable scan time and reproducibility this short-TE wbMRSI provides a method to map metabolite distributions over different brain regions of the whole human brain, indicating its potential applications.

Supplementary Material

Refer to Web version on PubMed Central for supplementary material.

References

1. Barker, PB.; Bizzi, A.; De Stefano, N.; Gullapalli, R.; LD, DM. Clinical MR Spectroscopy: Techniques and Applications. Cambridge University Press; 2009.
2. Spielman DM, Pauly JM, Macovski A, Glover GH, Enzmann DR. Lipid-suppressed single- and multisection proton spectroscopic imaging of the human brain. J Magn Reson Imaging. 1992; 2(3): 253–262. [PubMed: 1627859]
3. Ebel A, Govindaraju V, Maudsley AA. Comparison of inversion recovery preparation schemes for lipid suppression in 1H MRSI of human brain. Magn Reson Med. 2003; 49(5):903–908. [PubMed: 12704773]
4. Ebel A, Maudsley AA. Improved spectral quality for 3D MR spectroscopic imaging using a high spatial resolution acquisition strategy. Magn Reson Imaging. 2003; 21(2):113–120. [PubMed: 12670597]
5. Adalsteinsson E, Irarrazabal P, Topp S, Meyer C, Macovski A, Spielman DM. Volumetric spectroscopic imaging with spiral-based k-space trajectories. Magn Reson Med. 1998; 39(6):889–898. [PubMed: 9621912]
6. Ebel A, Dreher W, Leibfritz D. A fast variant of (1)H spectroscopic U-FLARE imaging using adjusted chemical shift phase encoding. J Magn Reson. 2000; 142(2):241–253. [PubMed: 10648140]
7. Mansfield P. Spatial mapping of the chemical shift in NMR. Magn Reson Med. 1984; 1(3):370–386. [PubMed: 6571566]
8. Posse S, DeCarli C, Le Bihan D. Three-dimensional echo-planar MR spectroscopic imaging at short echo times in the human brain. Radiology. 1994; 192(3):733–738. [PubMed: 8058941]
9. Zhu X, Ebel A, Ji JX, Schuff N. Spectral phase-corrected GRAPPA reconstruction of three-dimensional echo-planar spectroscopic imaging (3D-EPSI). Magn Reson Med. 2007; 57(5):815–820. [PubMed: 17457872]
10. Tsai SY, Otazo R, Posse S, Lin YR, Chung HW, Wald LL, Wiggins GC, Lin FH. Accelerated proton echo planar spectroscopic imaging (PEPSI) using GRAPPA with a 32-channel phased-array coil. Magn Reson Med. 2008; 59(5):989–998. [PubMed: 18429025]
11. Dydak U, Pruessmann KP, Weiger M, Tsao J, Meier D, Boesiger P. Parallel spectroscopic imaging with spin-echo trains. Magn Reson Med. 2003; 50(1):196–200. [PubMed: 12815695]
12. Gu M, Liu C, Spielman DM. Parallel spectroscopic imaging reconstruction with arbitrary trajectories using k-space sparse matrices. Magn Reson Med. 2009; 61(2):267–272. [PubMed: 19165883]
13. Sabati M, Zhan J, Govind V, Arheart KL, Maudsley AA. Impact of reduced k-space acquisition on pathologic detectability for volumetric MR spectroscopic imaging. J Magn Reson Imaging. 2014; 39(1):224–234. [PubMed: 23559504]

14. Gu M, Kim DH, Mayer D, Sullivan EV, Pfefferbaum A, Spielman DM. Reproducibility study of whole-brain 1H spectroscopic imaging with automated quantification. Magn Reson Med. 2008; 60(3):542–547. [PubMed: 18727040]
15. Maudsley AA, Domenig C, Sheriff S. Reproducibility of serial whole-brain MR spectroscopic imaging. NMR Biomed. 2010; 23(3):251–256. [PubMed: 19777506]
16. Hattingen E, Lanfermann H, Quick J, Franz K, Zanella FE, Pilatus U. 1H MR spectroscopic imaging with short and long echo time to discriminate glycine in glial tumours. MAGMA. 2009; 22(1):33–41. [PubMed: 18830648]
17. Wiedermann D, Schuff N, Matson GB, Soher BJ, Du AT, Maudsley AA, Weiner MW. Short echo time multislice proton magnetic resonance spectroscopic imaging in human brain: metabolite distributions and reliability. Magn Reson Imaging. 2001; 19(8):1073–1080. [PubMed: 11711231]
18. Tsai SY, Lin YR, Wang WC, Niddam DM. Short- and long-term quantitation reproducibility of brain metabolites in the medial wall using proton echo planar spectroscopic imaging. Neuroimage. 2012; 63(3):1020–1029. [PubMed: 22842213]
19. McLean MA, Woermann FG, Barker GJ, Duncan JS. Quantitative analysis of short echo time (1)H-MRSI of cerebral gray and white matter. Magn Reson Med. 2000; 44(3):401–411. [PubMed: 10975892]
20. Gasparovic C, Bedrick EJ, Mayer AR, Yeo RA, Chen H, Damaraju E, Calhoun VD, Jung RE. Test-retest reliability and reproducibility of short-echo-time spectroscopic imaging of human brain at 3T. Magn Reson Med. 2011; 66(2):324–332. [PubMed: 21360748]
21. Otazo R, Tsai SY, Lin FH, Posse S. Accelerated short-TE 3D proton echo-planar spectroscopic imaging using 2D-SENSE with a 32-channel array coil. Magn Reson Med. 2007; 58(6):1107–1116. [PubMed: 17968995]
22. Ebel A, Maudsley AA, Schuff N. Correction of local B0 shifts in 3D EPSI of the human brain at 4 T. Magn Reson Imaging. 2007; 25(3):377–380. [PubMed: 17371727]
23. Maudsley AA, Darkazanli A, Alger JR, Hall LO, Schuff N, Studholme C, Yu Y, Ebel A, Frew A, Goldgof D, Gu Y, Pagare R, Rousseau F, Sivasankaran K, Soher BJ, Weber P, Young K, Zhu X. Comprehensive processing, display and analysis for in vivo MR spectroscopic imaging. NMR Biomed. 2006; 19(4):492–503. [PubMed: 16763967]
24. Maudsley AA, Domenig C, Govind V, Darkazanli A, Studholme C, Arheart K, Bloomer C. Mapping of brain metabolite distributions by volumetric proton MR spectroscopic imaging (MRSI). Magn Reson Med. 2009; 61(3):548–559. [PubMed: 19111009]
25. Collins DL, Zijdenbos AP, Kollokian V, Sled JG, Kabani NJ, Holmes CJ, Evans AC. Design and construction of a realistic digital brain phantom. IEEE Trans Med Imaging. 1998; 17(3):463–468. [PubMed: 9735909]
26. Gigante AD, Bond DJ, Lafer B, Lam RW, Young LT, Yatham LN. Brain glutamate levels measured by magnetic resonance spectroscopy in patients with bipolar disorder: a meta-analysis. Bipolar Disord. 2012; 14(5):478–487. [PubMed: 22834460]
27. Gu M, Spielman DM. B1 and T1 insensitive water and lipid suppression using optimized multiple frequency-selective preparation pulses for whole-brain 1H spectroscopic imaging at 3T. Magn Reson Med. 2009; 61(2):462–466. [PubMed: 19161165]
28. Mullins PG, Chen H, Xu J, Caprihan A, Gasparovic C. Comparative reliability of proton spectroscopy techniques designed to improve detection of J-coupled metabolites. Magn Reson Med. 2008; 60(4):964–969. [PubMed: 18816817]
29. Pouwels PJ, Brockmann K, Kruse B, Wilken B, Wick M, Hanefeld F, Frahm J. Regional age dependence of human brain metabolites from infancy to adulthood as detected by quantitative localized proton MRS. Pediatr Res. 1999; 46(4):474–485. [PubMed: 10509371]
30. Provencher SW. Estimation of metabolite concentrations from localized in vivo proton NMR spectra. Magn Reson Med. 1993; 30(6):672–679. [PubMed: 8139448]
31. Keevil SF, Barbiroli B, Brooks JC, Cady EB, Canese R, Carlier P, Collins DJ, Gilligan P, Gobbi G, Hennig J, Kugel H, Leach MO, Metzler D, Mlynarik V, Moser E, Newbold MC, Payne GS, Ring P, Roberts JN, Rowland IJ, Thiel T, Tkac I, Topp S, Wittsack HJ, Podo F, et al. Absolute metabolite quantification by in vivo NMR spectroscopy: II. A multicentre trial of protocols for in vivo

localised proton studies of human brain. Magn Reson Imaging. 1998; 16(9):1093–1106. [PubMed: 9839993]

32. Scheidegger O, Wingeier K, Stefan D, Graveron-Demilly D, van Ormondt D, Wiest R, Slotboom J. Optimized quantitative magnetic resonance spectroscopy for clinical routine. Magn Reson Med. 2013; 70(1):25–32. [PubMed: 22907544]

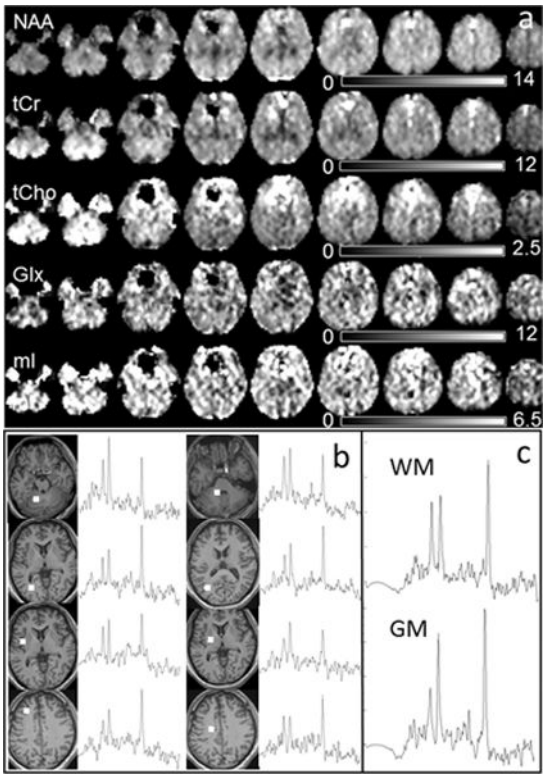

Fig. 1.

(a) Example metabolite maps of NAA, tCho, tCr, ml, and Glx, with every second axial slice shown at 11 mm spacing and displayed with intensity scales as indicated; (b) Example spectra of single voxels from white matter or gray matter in multiple brain regions as indicated on the T1 images; (c) Examples of averaged spectra from 8 voxels of white matter (top) and gray matter (bottom) respectively from the right parietal lobe.

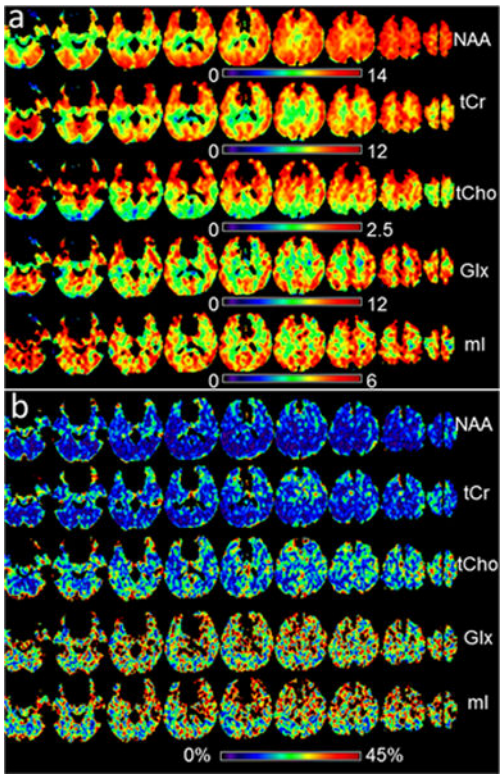

Fig. 2.

(a) Mean-value metabolite maps calculated from five repeated studies in standard space, with voxel exclusion criteria as described in the text, displayed with intensity scales as indicated; (b) The corresponding COV maps, displayed with an intensity scale between 0% to 45%.

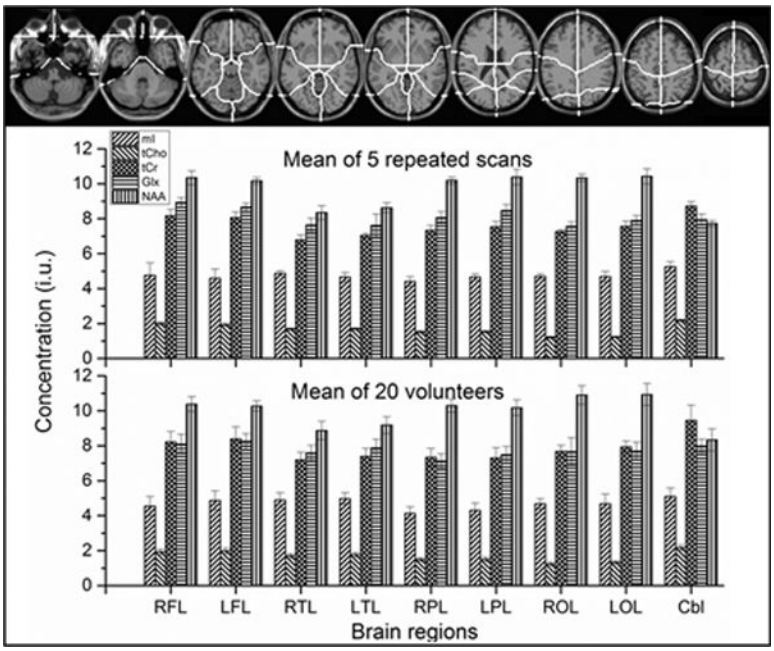

Fig. 3.

Mean regional metabolite concentrations of the 5 repeated scans (Fig.3 middle) and the 20 volunteers (Fig.3 bottom) obtained with multi-voxel analysis and linewidth threshold of 11 Hz, based on atlas-defined lobar anatomic regions which identified nine anatomical regions (Fig.3 top) defining the left and right cerebral lobes and the cerebellum (25). Note: the first letter R = right; the second letter F = frontal, P = parietal, O = occipital, T = temporal; the third letter L = lobe; Cbl = cerebellum.

Table 1

Mean metabolite concentrations and the results of tissue segmentation of the whole brain with associated intra-subject COVs for different linewidth thresholds, obtained with voxel-based analysis, averaged from 5 repeated scans (Top) and averaged among 20 volunteers (Bottom).

Metabolite or tissue type[1,2]	COV (%)			Concentration (i.u.)		
	LW threshold (Hz)			LW threshold (Hz)		
	8	11	13	8	11	13
NAA	12.79	13.73	15.99	9.82	9.84	9.59
tCho	19.30	19.86	22.32	1.71	1.74	1.89
tCr	14.45	15.10	16.72	7.75	7.84	7.96
Glx	30.58	31.13	30.57	8.20	8.25	8.30
ml	30.63	31.02	40.76	4.69	4.75	4.89
Tissue water	2.05	2.22	2.44			
LW	12.23	13.23	14.42	5.95	6.27	7.19
WM	5.50	5.56	5.50	0.48	0.47	0.45
GM	5.46	5.36	5.24	0.39	0.40	0.40
CSF	9.18	9.00	8.82	0.13	0.13	0.15

Metabolite or tissue type[3]	COV (%)			Concentration (i.u.)		
	LW threshold (Hz)			LW threshold (Hz)		
	8	11	13	8	11	13
NAA	18.48	19.36	23.37	9.95	10.02	9.73
tCho	24.87	24.81	34.04	1.71	1.78	1.91
tCr	20.23	20.79	25.71	7.99	8.13	8.21
Glx	35.25	35.33	40.04	7.82	7.87	7.89
ml	37.07	37.75	55.39	4.62	4.70	4.94
Tissue water	6.74	6.53	7.76			
LW	17.95	19.89	24.17	6.25	6.65	7.43
WM	20.44	20.71	21.05	0.46	0.47	0.44
GM	20.03	19.50	19.40	0.39	0.40	0.40
CSF	35.43	37.31	35.11	0.14	0.13	0.14

[1] CSF = cerebrospinal fluid, GM = gray matter, WM = white matter, LW = linewidth.

[2] Averaged from 5 repeated scans.

[3] Averaged among 20 volunteers.

Table 2

Mean metabolite concentrations of each brain region, in pure gray matter[1] and pure white matter[1] with associated standard deviation (SD) and ICC[2], averaged among the 20 volunteers

	RFL		LFL		RTL		LTL		RPL		LPL		ROL		LOL		Cbl		ICC
Brain regions	**Mean**	**SD**	**Mean**	**SD**	**Mean**	**SD**	**Mean**	**SD**	**Mean**	**SD**	**Mean**	**SD**	**Mean**	**SD**	**Mean**	**SD**	**Mean**	**SD**	
NAA	10.38	0.43	10.27	0.29	8.88	0.53	9.18	0.49	10.30	0.37	10.18	0.45	10.90	0.54	10.93	0.62	8.34	0.63	0.83
tCho	1.93	0.15	1.99	0.16	1.70	0.13	1.77	0.12	1.50	0.10	1.51	0.13	1.24	0.11	1.32	0.09	2.18	0.15	0.84
tCr	8.22	0.60	8.39	0.69	7.20	0.43	7.40	0.45	7.34	0.51	7.30	0.60	7.67	0.35	7.93	0.34	9.45	0.87	0.83
Glx	8.10	0.56	8.25	0.45	7.60	0.43	7.87	0.50	7.13	0.41	7.48	0.47	7.66	0.79	7.69	0.52	7.99	0.38	0.70
ml	4.54	0.55	4.87	0.54	4.89	0.42	4.98	0.33	4.13	0.37	4.29	0.42	4.67	0.30	4.68	0.56	5.09	0.49	0.87
pureGM																			
NAA	11.39	0.47	11.10	0.32	10.58	0.63	9.84	0.53	12.05	0.47	10.98	0.50	11.40	0.56	10.87	0.62	6.84	0.49	0.82
tCho	1.93	0.15	2.04	0.16	1.59	0.12	1.59	0.11	1.37	0.09	1.31	0.11	1.07	0.09	1.16	0.08	1.52	0.11	0.84
tCr	9.42	0.70	9.56	0.80	9.04	0.56	8.65	0.52	9.27	0.72	8.66	0.74	8.41	0.39	8.64	0.37	8.98	0.81	0.85
Glx	10.19	0.70	10.22	0.53	9.46	0.50	9.39	0.61	9.29	0.54	9.45	0.61	9.04	0.94	8.80	0.59	7.26	0.34	0.68
ml	5.24	0.64	5.79	0.64	5.65	0.49	5.52	0.37	4.86	0.46	4.90	0.48	5.02	0.33	4.66	0.55	3.49	0.33	0.88
pureWM																			
NAA	9.49	0.39	9.51	0.27	7.30	0.44	8.62	0.46	8.74	0.34	9.46	0.43	10.51	0.51	10.99	0.63	9.50	0.67	0.80
tCho	1.93	0.15	1.95	0.16	1.81	0.14	1.92	0.14	1.61	0.10	1.69	0.14	1.38	0.12	1.46	0.10	2.69	0.19	0.84
tCr	7.15	0.53	7.32	0.61	5.48	0.34	6.32	0.38	5.62	0.43	6.08	0.52	7.10	0.33	7.33	0.31	9.82	0.88	0.81
Glx	6.25	0.43	6.43	0.34	5.87	0.31	6.57	0.42	5.20	0.30	5.71	0.37	6.60	0.69	6.76	0.45	8.56	0.40	0.66
ml	3.93	0.48	4.02	0.45	4.18	0.36	4.51	0.30	3.48	0.33	3.75	0.37	4.40	0.28	4.70	0.56	6.33	0.59	0.86

[1]Generated by linear regression of the metabolite concentration against the normalized GM fraction of the lobe and extrapolating to pure GM or pure WM.

[2]ICC= the ratio of the variance of inter-subject metabolite distributions to the summation of the variance of inter-subject metabolite distributions, the variance of within subject metabolite distributions and the contribution of noise.